Available online at www.sciencedirect.com
SCIENCE DIRECT®
International Journal of Heat and Mass Transfer 47 (2004) 2123–2138
International Journal of HEAT and MASS TRANSFER
www.elsevier.com/locate/ijhmt

A numerical solution of composite heat transfer problems using meshless method

I.V. Singh *

Mechanical Engineering Group, Birla Institute of Technology and Science, Pilani 333031, Rajasthan, India

Received 8 August 2003; received in revised form 2 December 2003

Abstract

This paper deals with the three-dimensional numerical solution of composite heat transfer problems using meshless element free Galerkin method (EFG). The EFG method utilizes moving least square (MLS) approximants to approximate the unknown function of temperature $T(\mathbf{x})$ with $T^h(\mathbf{x})$. These MLS approximants are constructed by using a weight function, a basis function and a set of non-constants coefficients. Variational method is utilized for the discretization of the governing equations. The essential boundary conditions are enforced using Lagrange multiplier technique. The MATLAB codes have been developed to obtain the numerical solution. The EFG results are obtained for a model problem using different weight functions. Three new weight functions namely exponential, rational and cosine have been proposed. A comparison is made among the results obtained using proposed (exponential, rational and cosine) and existing (R&R, cubic spline, quartic spline, Gaussian, quadratic and hyperbolic) EFG weight functions with finite element method (FEM) for a three-dimensional composite heat transfer model problem. The validation of the EFG code has been achieved by comparing the EFG results with those obtained by FEM. The effect of scaling parameter on EFG results has also been discussed.

Keywords: Meshless method; Element free Galerkin method; Variational method; Lagrange multiplier technique; Three-dimensional heat transfer in composites

1. Introduction

The finite element method (FEM) is well-established numerical technique, which has been used to obtain the numerical solution of various problems in the areas of engineering and science. Although FEM is most general numerical method but the discretization, meshing and re-meshing of complex three-dimensional geometries of the problems are very rigorous and time-consuming process in comparison of assembly and solution of the finite element equations. Despite its numerous advantages, it is not well suited for certain classes of problems, such as crack propagation and moving discontinuities, solution of higher order partial differential equations, phase transformation, modeling of multi-scale phenomena, complex heat transfer problems and thermal analysis of turbine blades etc. To avoid these problems, recently a class of new methods has been developed, known as meshless methods. These methods include smooth particle hydrodynamics (SPH) [1], diffuse element method (DEM) [2], reproducing kernel particle method (RKPM) [3], partition of unity method [4], free mesh method [5], element free Galerkin (EFG) method [6–9], multiple scale kernel particle methods [10], Petrov–Galerkin diffuse element method (PG-DEM) [11], moving least square kernel Galerkin method [12], multiple scale meshfree methods [13], meshfree particle methods [14], local boundary integral equation (LBIE) method [15], meshless local Petrov–Galerkin (MLPG) method [16], natural element method [17], method of finite spheres [18] and natural neighbor Galerkin method [19]. Among all these

* Tel.: +91-1596-245073x259; fax: +91-1596-244183.
E-mail addresses: ivsingh@bits-pilani.ac.in, iv_singh@hotmail.com (I.V. Singh).

0017-9310/$ - see front matter
doi:10.1016/j.ijheatmasstransfer.2003.12.013

Nomenclature

$a_j(\mathbf{x})$	non-constant coefficients
c_{xI}, c_{yI}, c_{zI}	distances to the nearest neighbors in x, y and z directions
c	specific heat of the material
CS	cubic spline
QS	quartic spline
R&R	Rao and Rahman weight function
$d_{\max}$	scaling parameter
$\dot{Q}$	rate of internal heat generation/volume
h	convective heat transfer coefficient
k	coefficient of thermal conductivity
n	outward normal to the surface
$\bar{n}$	number of iterations
$p_j(\mathbf{x})$	monomial basis function
r_x, r_y, r_z	normalized radii along x, y and z directions
S_i	surfaces of three-dimensional models
$T^h(\mathbf{x})$	moving least square approximant
T_{S_i}	surface temperature
T_∞	surrounding fluid temperature
V	three-dimensional domain ($V_1 \cup V_2$)
x_I, y_I, z_I	coordinates of the Ith node
$w(\mathbf{x}-\mathbf{x}_I)$	weight function
λ	Lagrangian multiplier
$\Phi_I(\mathbf{x})$	shape function
ρ	density of the material

meshless methods, the EFG method has been successfully used to solve various types of problems in different areas such as fracture mechanics [20,21], static and dynamic fracture [22,23], wave and crack propagation [24,25], plates and shells [26,27], non-destructive testing [28], electromagnetic field [29], metal forming [30], heat transfer [31,32] and stochastic mechanics [33,34].

In this article, EFG method has been used to obtain the numerical solution of composite heat transfer problems. The steady state and transient analysis of the composite problems have been carried out in three-dimensional domain. In this method, function over the solution domain requires only a set of nodes. It does not require element connectivity like FEM. The integration over the solution domain requires only simple integration cell to obtain the solution. Variational method has been used for the discretization of the governing equations. The Lagrange multiplier method has been used to

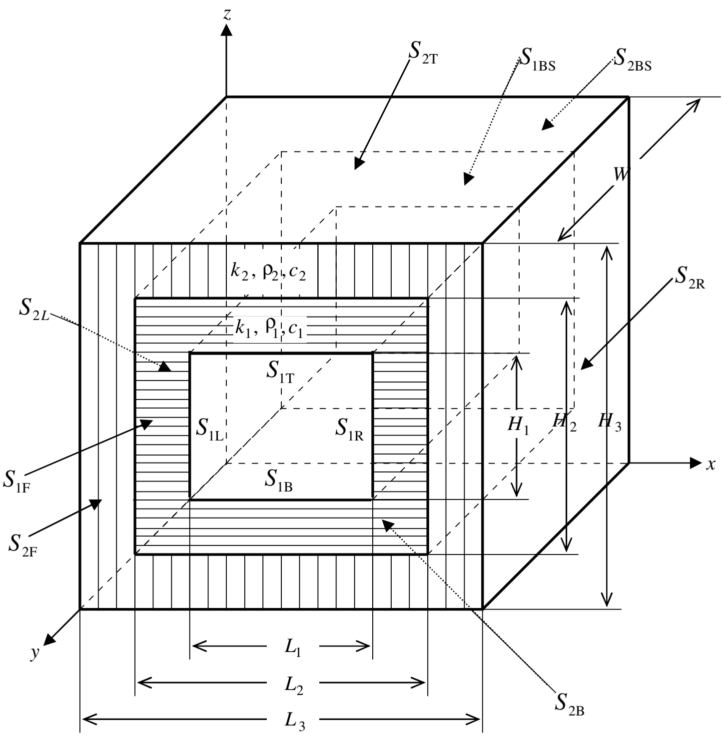

Fig. 1. Model for three-dimensional heat transfer in composites.

enforce the essential boundary conditions. The MATLAB codes have been developed to obtain the numerical solution. The EFG results are obtained using proposed and existing weight functions for a model problem and compared with those obtained by FEM.

2. The element free Galerkin method

The discretization of the governing equations by EFG method requires moving least square (MLS) approximants [35], which are made up of three components: a weight function associated with each node, a basis function and a set of non-constant coefficients.

2.1. Moving least square approximations

Using MLS approximation, the unknown function $T(\mathbf{x})$ is approximated by $T^h(\mathbf{x})$ over the domain [31,32]:

$$T^h(\mathbf{x}) = \sum_{j=1}^{m} p_j(\mathbf{x})a_j(\mathbf{x}) \equiv \mathbf{p}^{\mathrm{T}}(\mathbf{x})\mathbf{a}(x), \tag{1}$$

where, in 3-D,

$\mathbf{p}^{\mathrm{T}}(\mathbf{x}) = [1 \quad x \quad y \quad z]$.

$\mathbf{x}^{\mathrm{T}} = [x \quad y \quad z]$ and $\mathbf{P}^{\mathrm{T}}(\mathbf{x}) = \{p_1(\mathbf{x}), p_2(\mathbf{x}), \dots, p_m(\mathbf{x})\}$ is a vector of complete basis functions of order m, $\mathbf{a}(\mathbf{x}) = \{a_1(\mathbf{x}), a_2(\mathbf{x}), \dots, a_m(\mathbf{x})\}$ is a vector of unknown

Table 1
Data for three-dimensional heat transfer in composites

Parameters	Value of the parameters
Length (L_1)	0.20 m
Length (L_2)	0.40 m
Length (L_3)	0.60 m
Depth (W)	0.30 m
Height (H_1)	0.20 m
Height (H_2)	0.40 m
Height (H_3)	0.60 m
Thermal conductivity (k_1)	400 W/m °C
Thermal conductivity (k_2)	100 W/m °C
Specific heat of material 1 (c_1)	400 kJ/kg/K
Specific heat of material 2 (c_2)	300 kJ/kg/K
Density of material 1 (ρ_1)	10,000 kg/m^3
Density of material 2 (ρ_2)	8000 kg/m^3
Rate of internal heat generation in material 1 ($\dot{Q}_1$)	0.0
Rate of internal heat generation in material 2 ($\dot{Q}_2$)	0.0
Heat transfer coefficient (h)	200 W/m^2 °C
Initial temperature (T_{ini})	0
Time step size (Δt)	100 s
Surrounding fluid temperature (T_∞)	20 °C
Temperature ($T_{S_{1F}}$ and $T_{S_{2F}}$) at surfaces S_{1F} and S_{2F}	100 °C
Convection at all other surfaces	$-k\frac{\partial T}{\partial n'} = h(T - T_\infty)$, where $n' = x, y, z$

Table 2
Comparison of L_2-error norms for different EFG weight functions

Weight function	L_2-error norms			
	$d_{\max} = 1.01$		$d_{\max} = 1.51$	
	96 nodes	144 nodes	96 nodes	144 nodes
R&R	1.4135	0.4554	1.6044	0.7177
CS	1.6499	0.4807	1.7724	0.7299
QS	1.7014	0.4899	1.7759	0.8393
Gaussian	1.4097	0.4551	1.7381	0.7215
Quadratic	1.7683	0.5044	4.4778	3.6569
Hyperbolic	2.2073	0.6965	3.4691	2.7505
Exponential	1.7114	0.4935	1.7011	0.5169
Rational	1.7570	0.5003	1.6770	0.6804
Cosine	1.7655	0.5041	4.2802	3.4407

parameters that depends on $\mathbf{x}$ and m is the total number of terms in the basis. The coefficients $a_j(\mathbf{x})$ are obtained by minimizing the quadratic functional $J(\mathbf{x})$ given by

$$J(\mathbf{x}) = \sum_{I=1}^{n} w(\mathbf{x}-\mathbf{x}_I)\left\{\sum_{j=1}^{m} p_j(\mathbf{x}_I)a_j(\mathbf{x}) - T_I\right\}^2, \tag{2}$$

where $w(\mathbf{x}-\mathbf{x}_I)$ is a non-zero weight function and n is the number of nodes in the domain of influence. The minimization of $J(\mathbf{x})$ w.r.t. $a_j(\mathbf{x})$ leads the following set of equations:

$$\mathbf{A}(\mathbf{x})\mathbf{a}(\mathbf{x}) = \mathbf{B}(\mathbf{x})\mathbf{T}. \tag{3}$$

The above equation can be written as

$$\mathbf{a}(\mathbf{x}) = \mathbf{A}^{-1}(\mathbf{x})\mathbf{B}(\mathbf{x})\mathbf{T}, \tag{4}$$

where $\mathbf{A}$ and $\mathbf{B}$ are given as

$$\mathbf{A} = \sum_{I=1}^{n} w(\mathbf{x}-\mathbf{x}_I)\mathbf{p}(\mathbf{x}_I)\mathbf{p}^{\mathrm{T}}(\mathbf{x}_I), \tag{5}$$

$$\mathbf{B}(\mathbf{x}) = [w(\mathbf{x}-\mathbf{x}_1)\mathbf{p}(\mathbf{x}_1), w(\mathbf{x}-\mathbf{x}_2)\mathbf{p}(\mathbf{x}_2), \ldots, w(\mathbf{x}-\mathbf{x}_n)\mathbf{p}(\mathbf{x}_n)], \tag{6}$$

Table 3
Effect of scaling parameter on EFG results obtained using 96 nodes at the location ($x = 0.2$, $y = 0$ and $z = 0.2$)

Scaling parameter	Temperature (°C)								
	R&R	CS	QS	Gaussian	Quadratic	Hyperbolic	Exponential	Rational	Cosine
1.01	68.7599	69.6814	69.8559	68.7470	70.0992	71.2336	69.9146	70.2198	70.0872
1.11	68.8240	69.8749	69.9921	68.8647	69.7757	71.4085	69.8989	70.2053	69.7568
1.21	68.8637	69.9938	70.0532	69.0979	71.2776	71.4398	69.9467	70.2717	70.8908
1.31	68.9760	70.0390	70.0454	69.3489	72.0136	71.4634	69.9885	70.3435	71.5779
1.41	69.0642	70.0448	70.0531	69.5790	75.1559	68.8323	70.0702	70.3739	73.6472
1.51	69.1554	70.0358	70.0201	69.8325	66.2145	69.5592	70.1085	70.3975	68.8278
1.61	69.2582	70.0101	69.9105	70.0832	64.8373	70.3148	70.1450	70.4106	64.3830
1.71	69.3478	69.9574	69.7506	70.3014	84.8320	51.9305	70.1061	69.6094	84.8667
1.81	69.4230	69.8489	69.5147	70.5115	90.4010	49.7907	70.1183	69.3933	88.7365
1.91	69.4972	69.6746	69.2008	70.6956	85.8398	47.0927	70.1250	69.1041	85.9372
2.01	69.6197	69.4572	68.9415	70.9348	200.0383	−251.0259	70.2386	69.2368	179.9973
2.11	69.7541	69.2840	69.1168	71.1634	54.9363	−46.0624	70.3317	69.5501	68.3182
2.21	69.8994	69.2761	70.1341	71.3831	45.7752	−49.8714	70.3384	69.0438	49.4954
2.31	70.0324	69.5819	72.2938	71.6377	27.6879	−52.0982	70.3370	68.3591	23.7556
2.41	70.2208	70.4023	75.8669	72.2316	90.3990	60.2864	70.3883	71.1334	65.7887

Table 4
Effect of scaling parameter on EFG results obtained using 144 nodes at the location ($x = 0.2$, $y = 0$ and $z = 0.2$)

Scaling parameter	Temperature (°C)								
	R&R	CS	QS	Gaussian	Quadratic	Hyperbolic	Exponential	Rational	Cosine
1.01	69.5283	69.7622	69.8002	69.5263	69.8810	70.4315	69.8285	69.9945	69.8725
1.11	69.5298	69.8133	69.8402	69.5272	69.2691	71.1781	69.7805	69.9000	69.4062
1.21	69.5061	69.8488	69.8601	69.5828	70.0406	71.5128	69.7957	69.9321	69.9690
1.31	69.5252	69.8477	69.8373	69.6441	70.7989	71.8830	69.8116	69.9670	70.4416
1.41	69.5310	69.8315	69.8210	69.6889	72.6063	68.1916	69.8558	69.9003	69.1976
1.51	69.5365	69.8073	69.7664	69.7414	77.2801	68.3606	69.8714	69.8784	69.2338
1.61	69.5466	69.7617	69.6445	69.7833	79.6075	68.6813	69.8846	69.8470	74.8385
1.71	69.5555	69.6827	69.4703	69.7977	89.9595	98.6489	69.8745	69.4805	93.9422
1.81	69.5636	69.5572	69.2433	69.7760	95.1976	104.0035	69.8739	69.3316	96.4449
1.91	69.5672	69.3805	68.9537	69.6921	109.7309	108.5163	69.8681	69.1498	116.5362
2.01	69.6230	69.1639	68.6529	69.6113	115.7373	−263.4159	70.0389	69.6027	−9.9285
2.11	69.7080	68.9530	68.5170	69.4219	26.8723	−85.4597	70.1149	69.8908	5.0000
2.21	69.7996	68.7924	68.6821	69.0756	−36.1904	−102.3341	70.1253	69.5818	−31.000
2.31	69.8821	68.7127	69.1719	68.5567	−95.9047	−116.5132	70.1299	69.1700	−89.000
2.41	70.0084	68.7614	70.0248	68.0867	−181.4461	−12.8605	70.1654	70.5231	−25.000

$$\mathbf{T}^{\mathrm{T}} = [T_1, T_2, \ldots, T_n]. \tag{7}$$

Substituting Eq. (5) in Eq. (1), the MLS approximants is obtained as

$$T^h(\mathbf{x}) = \sum_{I=1}^{n} \Phi_I(\mathbf{x}) T_I = \mathbf{\Phi}(\mathbf{x})\mathbf{T}, \tag{8}$$

where shape function $\Phi_I(\mathbf{x})$ is defined as

$$\Phi_I(\mathbf{x}) = \sum_{j=0}^{m} p_j(\mathbf{x})(\mathbf{A}^{-1}(\mathbf{x})\mathbf{B}(\mathbf{x}))_{jI} = \mathbf{p}^{\mathrm{T}}\mathbf{A}^{-1}\mathbf{B}_I. \tag{9}$$

The derivative of the shape function is given as

$$\begin{aligned}\Phi_{I,\mathbf{x}}(\mathbf{x}) &= (\mathbf{p}^{\mathrm{T}}\mathbf{A}^{-1}\mathbf{B}_I)_{,x} \\ &= \mathbf{p}^{\mathrm{T}}_{,x}\mathbf{A}^{-1}\mathbf{B}_I + \mathbf{p}^{\mathrm{T}}(\mathbf{A}^{-1})_{,x}\mathbf{B}_I + \mathbf{p}^{\mathrm{T}}\mathbf{A}^{-1}(\mathbf{B}_I)_{,x}.\end{aligned} \tag{10}$$

2.2. The weight function

The weight function is non-zero over a small neighborhood of a node $\mathbf{x}_I$, called the support of node I. The choice of weight function $w(\mathbf{x} - \mathbf{x}_I)$ affects the resulting approximation $T^h(\mathbf{x}_I)$. The smoothness of the

Table 5
Effect of scaling parameter on EFG results obtained using 96 nodes at the location ($x = 0.5$, $y = 0$ and $z = 0.1$)

Scaling parameter	Temperature (°C)								
	R&R	CS	QS	Gaussian	Quadratic	Hyperbolic	Exponential	Rational	Cosine
1.01	65.2240	65.2701	65.2947	65.2220	65.3966	66.6384	65.3127	65.3881	65.3797
1.11	65.4560	65.1918	65.2405	65.5338	63.7792	67.1631	65.6373	65.8368	64.0212
1.21	65.5982	65.2858	65.4674	65.6081	66.3749	67.3492	65.6630	65.8743	66.1522
1.31	65.6333	65.6026	65.7462	65.6758	67.2630	67.5354	65.6843	65.9174	66.8925
1.41	65.7796	65.8024	65.9591	65.8897	66.7333	71.2317	65.4776	66.4089	65.3792
1.51	65.9391	66.0662	66.4053	66.0943	69.4435	71.5153	65.5851	66.6257	69.3822
1.61	66.0838	66.4183	66.9129	66.3601	69.4305	71.6664	65.7031	66.8425	69.6526
1.71	66.3264	66.8159	67.3803	66.8256	71.4900	130.7711	66.2410	68.8733	66.7970
1.81	66.6525	67.3083	67.9771	67.3176	90.6450	139.1832	66.4477	69.3915	80.6481
1.91	66.9694	67.8812	68.7169	67.9129	106.4591	145.6547	66.6645	69.9561	97.3552
2.01	67.4527	68.5268	69.5909	68.7957	309.6332	200.9514	67.2940	71.9022	199.4708
2.11	67.9424	69.2744	70.6811	69.7938	97.6029	127.2347	67.6313	72.5475	99.1303
2.21	68.4410	70.1919	72.2049	71.0345	115.5707	118.9625	67.9229	73.3246	104.3752
2.31	68.9379	71.3712	74.4090	72.6151	110.3517	110.2966	68.2219	74.1727	88.2042
2.41	69.4961	72.9380	77.5522	74.6972	364.0192	97.9427	68.6005	75.1589	301.0513

Table 6
Effect of scaling parameter on EFG results obtained using 144 nodes at the location ($x = 0.5$, $y = 0$ and $z = 0.1$)

Scaling parameter	Temperature (°C)								
	R&R	CS	QS	Gaussian	Quadratic	Hyperbolic	Exponential	Rational	Cosine
1.01	65.7839	65.4975	65.4281	65.7886	65.3323	64.9817	65.4118	65.3726	65.3352
1.11	65.9692	65.3358	65.2977	66.0157	63.2457	65.9025	65.6425	65.6599	63.6647
1.21	66.0552	65.3573	65.4582	65.9827	64.9190	66.0568	65.6372	65.6537	64.9879
1.31	66.0320	65.5705	65.6501	65.9315	65.4741	66.2459	65.6339	65.6462	65.3163
1.41	66.1040	65.6928	65.7440	65.9897	64.1941	67.0919	65.4166	65.8207	62.7500
1.51	66.1780	65.8320	65.9509	66.0163	63.0606	68.0141	65.4694	65.9133	61.6468
1.61	66.2327	65.9802	66.1070	66.0686	74.7428	68.7068	65.5277	65.9951	67.2945
1.71	66.3732	66.0950	66.1346	66.2590	75.9779	81.2125	65.9008	67.1506	79.4287
1.81	66.5845	66.2018	66.1314	66.4340	81.7540	85.7784	66.0172	67.3286	75.7092
1.91	66.7791	66.2689	66.0590	66.6520	101.9692	90.6335	66.1367	67.4975	99.3016
2.01	67.1134	66.2588	65.8512	67.0619	103.8000	−17.6972	66.6484	68.5127	−200.270
2.11	67.4649	66.1487	65.4883	67.5020	−196.100	33.8821	66.8697	68.9848	−150.00
2.21	67.8114	65.9482	65.0684	68.0334	−360.000	39.0119	67.0414	69.1034	−240.00
2.31	68.1467	65.6617	64.6482	68.7079	−273.900	44.8138	67.2115	69.1808	−340.00
2.41	68.5149	65.2763	64.2434	69.6594	−2403.80	−11.4020	67.4767	69.8681	−290.00

shape function is governed by the smoothness of weight function. Therefore the selection of appropriate weight function is essential in EFG method. The different weight functions used in present analysis are written as a function of normalized radius r as

Rao and Rahman (R&R) weight function [40]

$$w(\mathbf{x}-\mathbf{x}_I)=w(r)=\left\{\begin{array}{ll}\frac{(1+\beta^2r^2)^{-((1+\beta)/2)}-(1+\beta^2)^{-((1+\beta)/2)}}{1-(1+\beta^2)^{-((1+\beta)/2)}} & r\leqslant 1\\ 0 & r>1\end{array}\right\}. \tag{11a}$$

The cubic spline (CS) weight function [8]

$$w(\mathbf{x}-\mathbf{x}_I)=w(r)=\left\{\begin{array}{ll}\frac{2}{3}-4r^2+4r^3 & r\leqslant\frac{1}{2}\\ \frac{4}{3}-4r+4r^2-\frac{4}{3}r^3 & \frac{1}{2}<r\leqslant 1\\ 0 & r>1\end{array}\right\}. \tag{11b}$$

The quartic spline (QS) weight function [8]

$$w(\mathbf{x}-\mathbf{x}_I)=w(r)=\left\{\begin{array}{ll}1-6r^2+8r^3-3r^4 & 0\leqslant r\leqslant 1\\ 0 & r>1\end{array}\right\}. \tag{11c}$$

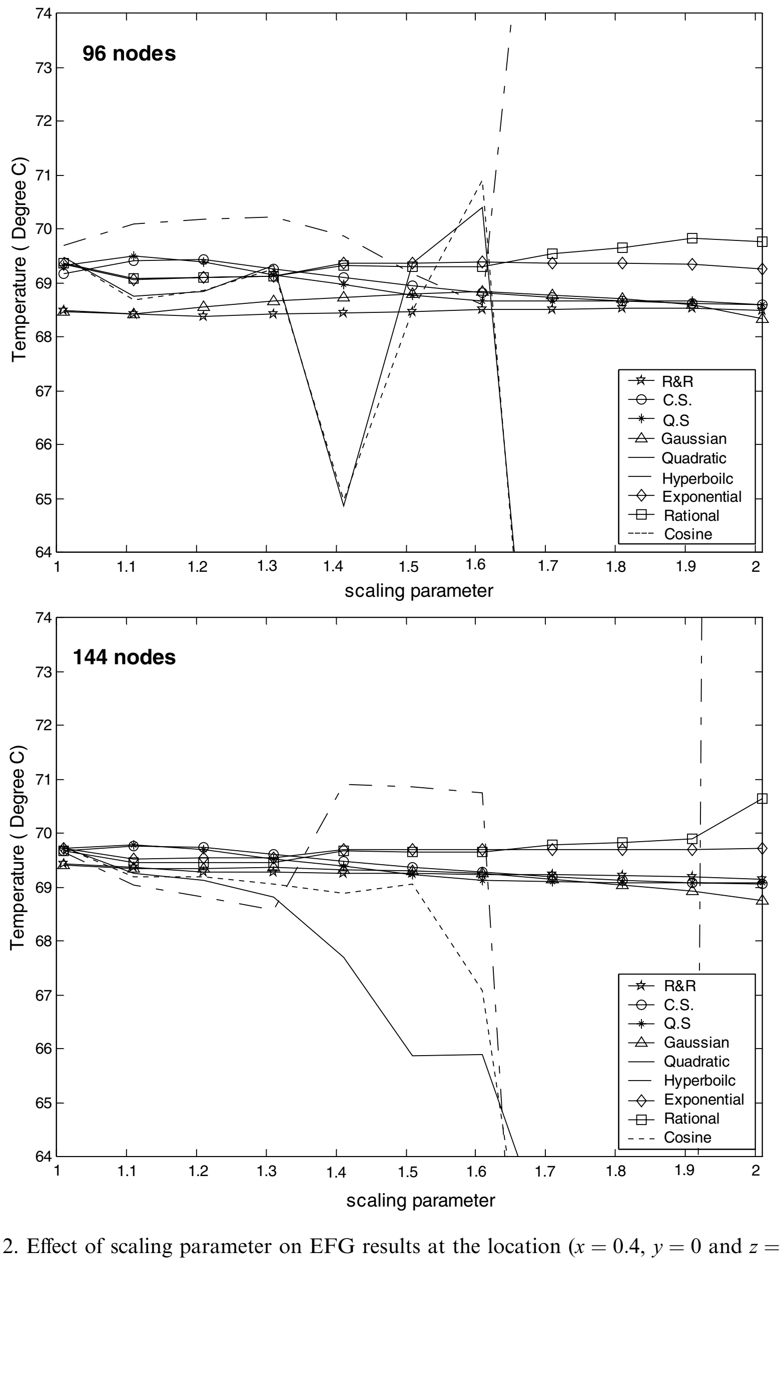

Fig. 2. Effect of scaling parameter on EFG results at the location ($x = 0.4$, $y = 0$ and $z = 0.3$).

Gaussian weight function [8]

$$w(\mathbf{x}-\mathbf{x}_I) = w(r) = \left\{ \begin{array}{ll} e^{-(2.5r)^2} & 0 \leqslant r \leqslant 1 \\ 0 & r > 1 \end{array} \right\}. \quad (11d)$$

The quadratic weight function [36]

$$w(\mathbf{x}-\mathbf{x}_I) = w(r) = \left\{ \begin{array}{ll} 1-r^2 & 0 \leqslant r \leqslant 1 \\ 0 & r > 1 \end{array} \right\}. \quad (11e)$$

The hyperbolic weight function [32]

$$w(\mathbf{x}-\mathbf{x}_I) = w(r) = \left\{ \begin{array}{ll} \mathrm{sech}(r+3) & 0 \leqslant r \leqslant 1 \\ 0 & r > 1 \end{array} \right\}. \quad (11f)$$

The exponential weight function

$$w(\mathbf{x}-\mathbf{x}_I) = w(r) = \left\{ \begin{array}{ll} 100^{-r} & 0 \leqslant r \leqslant 1 \\ 0 & r > 1 \end{array} \right\}. \quad (11g)$$

The rational weight function

$$w(\mathbf{x}-\mathbf{x}_I) = w(r) = \left\{ \begin{array}{ll} \frac{1}{r^2+0.1} & 0 \leqslant r \leqslant 1 \\ 0 & r > 1 \end{array} \right\}. \quad (11h)$$

The cosine weight function

$$w(\mathbf{x}-\mathbf{x}_I) = w(r) = \left\{ \begin{array}{ll} \cos\left(\frac{\pi r}{2}\right) & 0 \leqslant r \leqslant 1 \\ 0 & r > 1 \end{array} \right\}, \quad (11i)$$

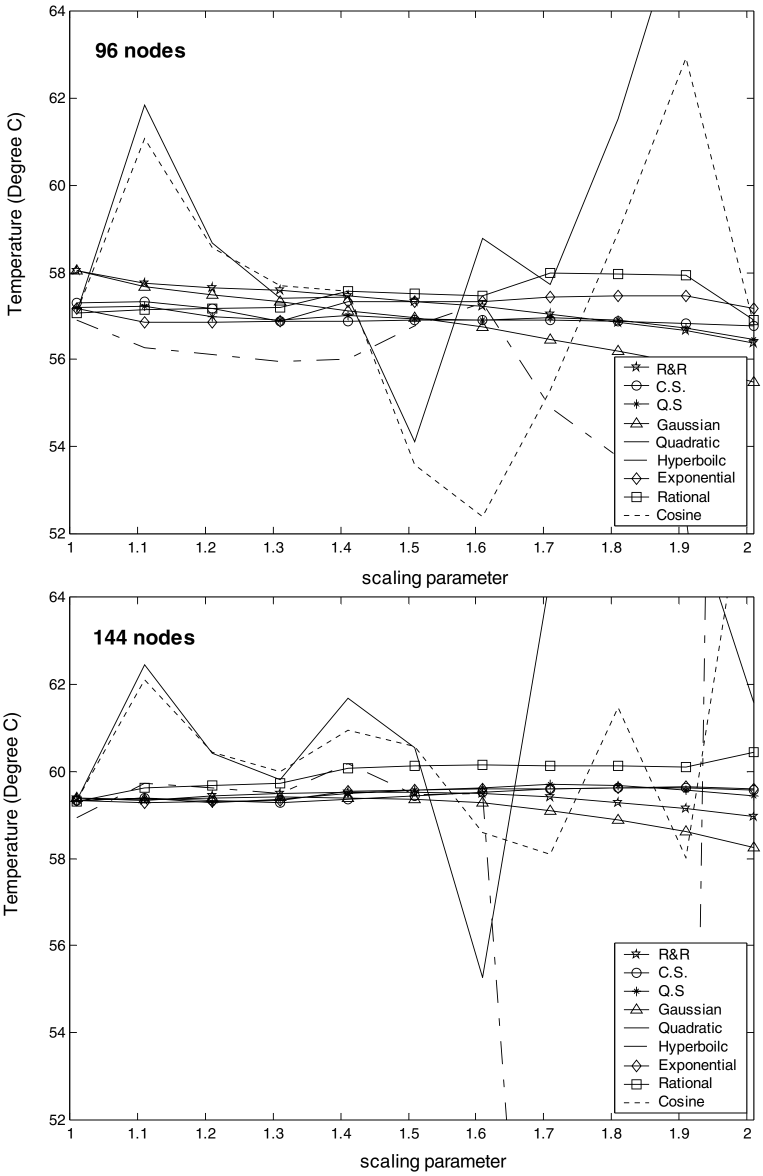

Fig. 3. Effect of scaling parameter on EFG results at the location ($x = 0.6$, $y = 0$ and $z = 0.3$).

where

$$(r)_I = \frac{\|\mathbf{x} - \mathbf{x}_I\|}{d_{mI}}, \quad (r_x)_I = \frac{\|x - x_I\|}{d_{mxI}},$$

$$(r_y)_I = \frac{\|y - y_I\|}{d_{myI}}, \quad (r_z)_I = \frac{\|z - z_I\|}{d_{mzI}}.$$

$$d_{mxI} = d_{\max}c_{xI}, d_{myI} = d_{\max}c_{yI}, d_{mzI} = d_{\max}c_{zI}.$$

$d_{\max}$ is the scaling parameter and β is a parameter which controls the shape of the weight function. c_{xI}, c_{yI} and c_{zI} at node I, are the distances to the nearest neighbors. d_{mxI}, d_{myI} and d_{mzI} are chosen such that the matrix is non-singular everywhere in the domain.

The weight function at any given point is obtained as

$$w(\mathbf{x} - \mathbf{x}_I) = w(r_x)w(r_y)w(r_z) = w_x w_y w_z, \tag{12}$$

where $w(r_x)$, $w(r_y)$ and $w(r_z)$ can be calculated by replacing r by r_x, r_y and r_z in the expression of $w(r)$.

The derivatives of the weight function are obtained as

$$w_{,x} = \frac{\mathrm{d}w_x}{\mathrm{d}x} w_y w_z, \quad w_{,y} = \frac{\mathrm{d}w_y}{\mathrm{d}y} w_x w_z \quad \text{and}$$

$$w_{,z} = \frac{\mathrm{d}w_z}{\mathrm{d}z} w_x w_y. \tag{13}$$

2.3. Enforcement of essential boundary conditions

Lack of Kronecker delta property in EFG shape functions Φ_I poses some difficulty in the imposition of essential boundary conditions. For that different numerical techniques have been proposed to enforce the essential boundary conditions in EFG method such as Lagrange multiplier technique [31,32], modified variational principle approach [7], penalty approach [37], coupling with FEM [38], singular weight function approach [39] and transformation technique [40] etc. In the present work, Lagrange multiplier technique is used to

Table 7
Comparison of EFG results obtained using 96 nodes with FEM at the location ($x = 0.4$, $y = 0$ and $z = 0.2$) for $d_{\max} = 1.01$

Time (s)×10^2	Temperature (°C)									
	$d_{\max} = 1.01$									FEM
	R&R	CS	QS	Gaussian	Quadratic	Hyperbolic	Exponential	Rational	Cosine	
0	0.0000	0.0000	0.0000	0.0000	0.0000	0.0000	0.0000	0.0000	0.0000	0.0000
3	24.4552	25.3345	25.5048	24.4405	25.7137	26.5095	25.5403	25.7261	25.7058	37.9128
6	51.5073	52.4294	52.6056	51.4934	52.8404	53.8647	52.6560	52.9196	52.8300	55.2100
9	62.0205	62.9407	63.1156	62.0072	63.3553	64.4474	63.1709	63.4602	63.3439	63.6469
12	66.1263	67.0460	67.2204	66.1132	67.4620	68.5795	67.2777	67.5766	67.4502	67.8024
15	67.7307	68.6509	68.8253	67.7177	69.0677	70.1954	68.8834	69.1861	69.0559	69.8543
18	68.3577	69.2785	69.4529	68.3448	69.6958	70.8274	69.5113	69.8155	69.6838	70.8682
21	68.6027	69.5239	69.6983	68.5898	69.9414	71.0747	69.7569	70.0617	69.9295	71.3693
24	68.6985	69.6198	69.7943	68.6856	70.0375	71.1714	69.8530	70.1580	70.0255	71.6170
27	68.7359	69.6573	69.8318	68.7230	70.0751	71.2093	69.8905	70.1956	70.0631	71.7395
30	68.7506	69.6720	69.8465	68.7376	70.0898	71.2241	69.9052	70.2103	70.0778	71.8000

Table 8
Comparison of EFG results obtained using 96 nodes with FEM at the location ($x = 0.4$, $y = 0$ and $z = 0.2$) for $d_{\max} = 1.51$

Time (s)×10^2	Temperature (°C)									
	$d_{\max} = 1.51$									FEM
	R&R	CS	QS	Gaussian	Quadratic	Hyperbolic	Exponential	Rational	Cosine	
0	0.0000	0.0000	0.0000	0.0000	0.0000	0.0000	0.0000	0.0000	0.0000	0.0000
3	24.9723	25.8472	25.9543	25.6531	34.2501	23.5621	25.7571	26.0760	36.2574	37.9128
6	51.9380	52.8428	52.8721	52.6407	53.7453	51.5526	52.8619	53.1690	56.1387	55.2100
9	62.4209	63.3134	63.3141	63.1110	61.3292	62.5171	63.3696	63.6672	63.8565	63.6469
12	66.5198	67.4053	67.3956	67.2026	64.3003	66.8053	67.4734	67.7663	66.8793	67.8024
15	68.1239	69.0063	68.9928	68.8034	65.4645	68.4823	69.0779	69.3687	68.0641	69.8543
18	68.7517	69.6329	69.6180	69.4298	65.9206	69.1381	69.7054	69.9952	68.5284	70.8682
21	68.9974	69.8781	69.8627	69.6749	66.0993	69.3946	69.9508	70.2402	68.7105	71.3693
24	69.0936	69.9741	69.9585	69.7708	66.1694	69.4948	70.0468	70.3360	68.7818	71.6170
27	69.1312	70.0116	69.9960	69.8084	66.1968	69.5340	70.0844	70.3734	68.8098	71.7395
30	69.1460	70.0263	70.0107	69.8231	66.2075	69.5494	70.0990	70.3881	68.8208	71.8000

enforce the essential boundary conditions due to its simplicity and accuracy.

In 3-D, Lagrange multiplier λ is expressed as

$$\lambda(\mathbf{x}) = N_I(a)\lambda_I, \quad \mathbf{x} \in S, \tag{14a}$$

$$\delta\lambda(\mathbf{x}) = N_I(a)\delta\lambda_I, \quad \mathbf{x} \in S, \tag{14b}$$

where $N_I(a)$ is a Lagrange interpolant and a is the area for the essential boundary conditions.

3. Implementation of the EFG method

A general form of energy equation for three-dimensional heat transfer in isotropic materials with thermal properties independent of temperature is given as

$$k\left(\frac{\partial^2 T}{\partial x^2} + \frac{\partial^2 T}{\partial y^2} + \frac{\partial^2 T}{\partial z^2}\right) + \dot{Q} = \rho c \dot{T}. \tag{15a}$$

The initial conditions are given as at time $t = 0$

$$T = T_{\text{ini}} \quad \text{on } V. \tag{15b}$$

The essential boundary conditions are given as

at the front surface of material 1 (S_{1F}), $y = W$,

$$T = T_{1F}; \tag{15c}$$

at the front surface of material 2 (S_{2F}), $y = W$,

$$T = T_{2F}. \tag{15d}$$

The natural boundary conditions are given as

at the back surface of material 1 and 2 (S_{1BS} and S_{2BS}),

$$-k\frac{\partial T}{\partial y} n_y = h(T - T_\infty); \tag{15e}$$

Table 9

Comparison of temperature value obtained using 144 nodes with FEM at the location ($x = 0.4$, $y = 0$ and $z = 0.2$) for $d_{\max} = 1.01$

Time (s)×10^2	Temperature (°C)									
	$d_{\max} = 1.01$									FEM
	R&R	CS	QS	Gaussian	Quadratic	Hyperbolic	Exponential	Rational	Cosine	
0	0.0000	0.0000	0.0000	0.0000	0.0000	0.0000	0.0000	0.0000	0.0000	0.0000
3	27.7469	27.7777	27.7756	27.7462	27.7800	27.7289	27.7804	27.7987	27.7775	31.0311
6	50.9534	51.1260	51.1522	50.9515	51.2070	51.5229	51.1714	51.2790	51.2011	52.1403
9	61.3727	61.5773	61.6096	61.3708	61.6785	62.1247	61.6339	61.7744	61.6712	61.9275
12	65.9488	66.1682	66.2034	65.9469	66.2786	66.7820	66.2298	66.3846	66.2705	66.5053
15	67.9572	68.1840	68.2206	67.9553	68.2988	68.8280	68.2481	68.4091	68.2905	68.6377
18	68.8387	69.0692	69.1065	68.8368	69.1861	69.7269	69.1344	69.2982	69.1777	69.6303
21	69.2257	69.4579	69.4956	69.2237	69.5758	70.1219	69.5237	69.6887	69.5673	70.0923
24	69.3955	69.6286	69.6664	69.3935	69.7470	70.2954	69.6947	69.8602	69.7385	70.3073
27	69.4700	69.7035	69.7415	69.4680	69.8222	70.3717	69.7697	69.9355	69.8136	70.4074
30	69.5027	69.7365	69.7744	69.5008	69.8552	70.4052	69.8027	69.9686	69.8467	70.4539

Table 10

Comparison of temperature value obtained using 144 nodes with FEM at the location ($x = 0.4$, $y = 0$ and $z = 0.2$) for $d_{\max} = 1.51$

Time (s)×10^2	Temperature (°C)									
	$d_{\max} = 1.51$									FEM
	R&R	CS	QS	Gaussian	Quadratic	Hyperbolic	Exponential	Rational	Cosine	
0	0.0000	0.0000	0.0000	0.0000	0.0000	0.0000	0.0000	0.0000	0.0000	0.0000
3	28.9342	28.5827	28.7961	28.6839	36.4238	8.6876	27.6985	27.2910	34.0727	31.0311
6	50.8937	51.1169	51.0966	51.0776	59.7803	42.9939	51.2045	51.1816	53.7799	52.1403
9	61.1118	61.4391	61.3686	61.3700	69.6179	57.4475	61.6850	61.7254	62.4151	61.9275
12	65.7326	66.0621	65.9906	65.9884	73.9208	63.6642	66.2814	66.3225	66.2236	66.5053
15	67.8190	68.1311	68.0687	68.0588	75.8071	66.3394	68.2970	68.3274	67.9048	68.6377
18	68.7610	69.0571	69.0030	68.9871	76.6342	67.4907	69.1809	69.2019	68.6470	69.6303
21	69.1863	69.4715	69.4231	69.4032	76.9969	67.9862	69.5686	69.5833	68.9747	70.0923
24	69.3784	69.6570	69.6120	69.5898	77.1559	68.1995	69.7386	69.7497	69.1194	70.3073
27	69.4651	69.7400	69.6970	69.6734	77.2257	68.2912	69.8131	69.8223	69.1833	70.4074
30	69.5042	69.7772	69.7352	69.7109	77.2563	68.3307	69.8458	69.8540	69.2115	70.4539

at the inner and outer surfaces of materials 1 and 2,

$$-k\frac{\partial T}{\partial n'}n_{n'} = h(T - T_\infty). \tag{15f}$$

The compatibility requirements at the interface of two materials are given as

$$-k\left(\frac{\partial T}{\partial n'}\right)\bigg|_{\text{mat1}} = -k\left(\frac{\partial T}{\partial n'}\right)\bigg|_{\text{mat2}}, \tag{15g}$$

where $n_{n'}$ is the cosine of angle between n and n', n is the outward normal to the surface and $n' = x, z$.

The weighted integral form of Eq. (15a) is obtained as

$$\int_V w\left[k\left(\frac{\partial^2 T}{\partial x^2} + \frac{\partial^2 T}{\partial y^2} + \frac{\partial^2 T}{\partial z^2}\right) + \dot{Q} - \rho c\dot{T}\right]\mathrm{d}V = 0. \tag{16}$$

The weak form of Eq. (16) will be

$$\int_V [k(\nabla^{\mathrm{T}} w)\nabla T - w\dot{Q} + w\rho c\dot{T}]\,\mathrm{d}V - \int_S wk\left(\frac{\partial T}{\partial x}n_x + \frac{\partial T}{\partial y}n_y + \frac{\partial T}{\partial z}n_z\right)\mathrm{d}S = 0. \tag{17}$$

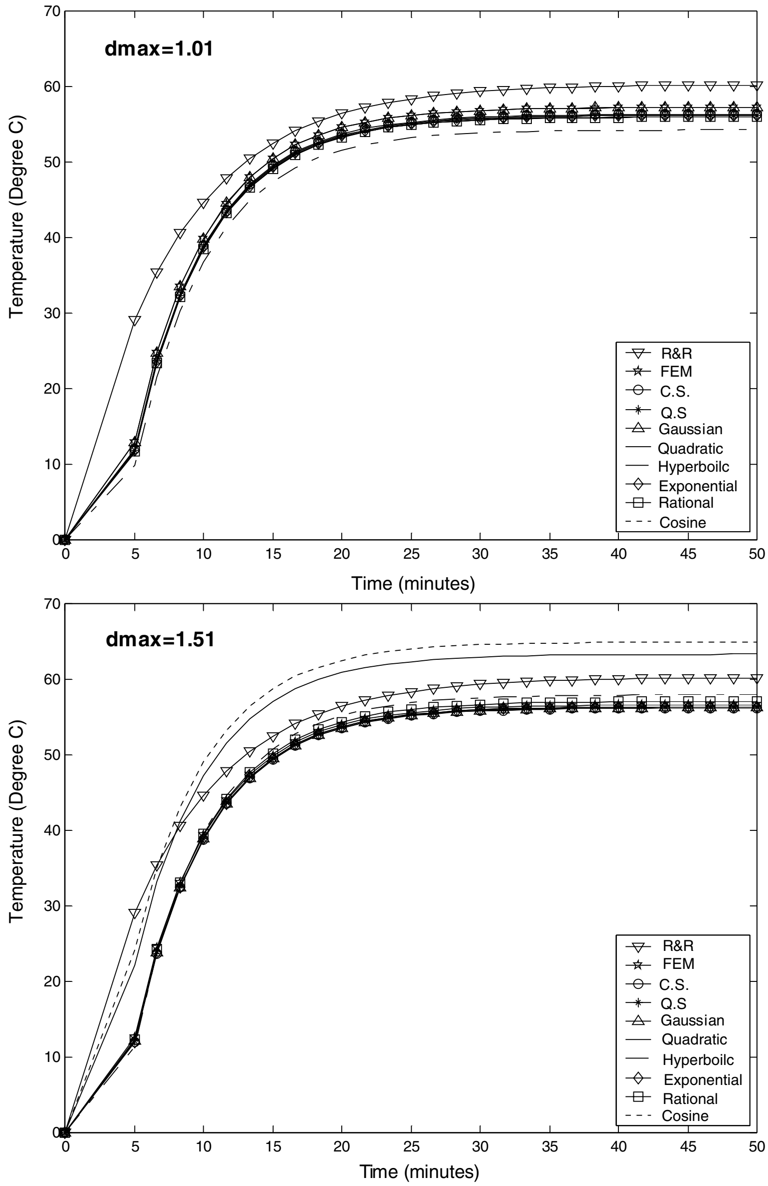

Fig. 4. Comparison of EFG results obtained using 96 nodes with FEM at the location ($x = 0.6$, $y = 0$ and $z = 0.2$).

Introducing natural boundary conditions in weak form, Eq. (17) reduces to

$$\sum_{i=1}^{2}\int_{V_i}[k_i(\nabla^{\mathrm{T}}w)\nabla T - w\dot{Q}_i + w\rho_i c_i\dot{T}]\,\mathrm{d}V + \sum_{j=1}^{10}\int_{S_j} wh(T-T_\infty)\,\mathrm{d}S = 0, \tag{18}$$

where

$$\nabla^{\mathrm{T}} = \begin{bmatrix}\frac{\partial}{\partial x} & \frac{\partial}{\partial y} & \frac{\partial}{\partial z}\end{bmatrix}$$

and

$S_1 = S_{1L}$, $S_2 = S_{2L}$, $S_3 = S_{1R}$, $S_4 = S_{2R}$, $S_5 = S_{1B}$, $S_6 = S_{2B}$, $S_7 = S_{1T}$, $S_8 = S_{2T}$, $S_9 = S_{1\mathrm{BS}}$, $S_{10} = S_{2\mathrm{BS}}$.

The functional $I(T)$ can be written as

$$I(T) = \sum_{i=1}^{2}\int_{V_i}\left[\frac{1}{2}k_i(\nabla^{\mathrm{T}}T)\nabla T - T\dot{Q}_i + \rho_i c_i T\dot{T}\right]\mathrm{d}V + \sum_{j=1}^{10}\int_{S_j}\frac{hT^2}{2}\,\mathrm{d}S - \sum_{j=1}^{10}\int_{S_j} hTT_\infty\,\mathrm{d}S. \tag{19}$$

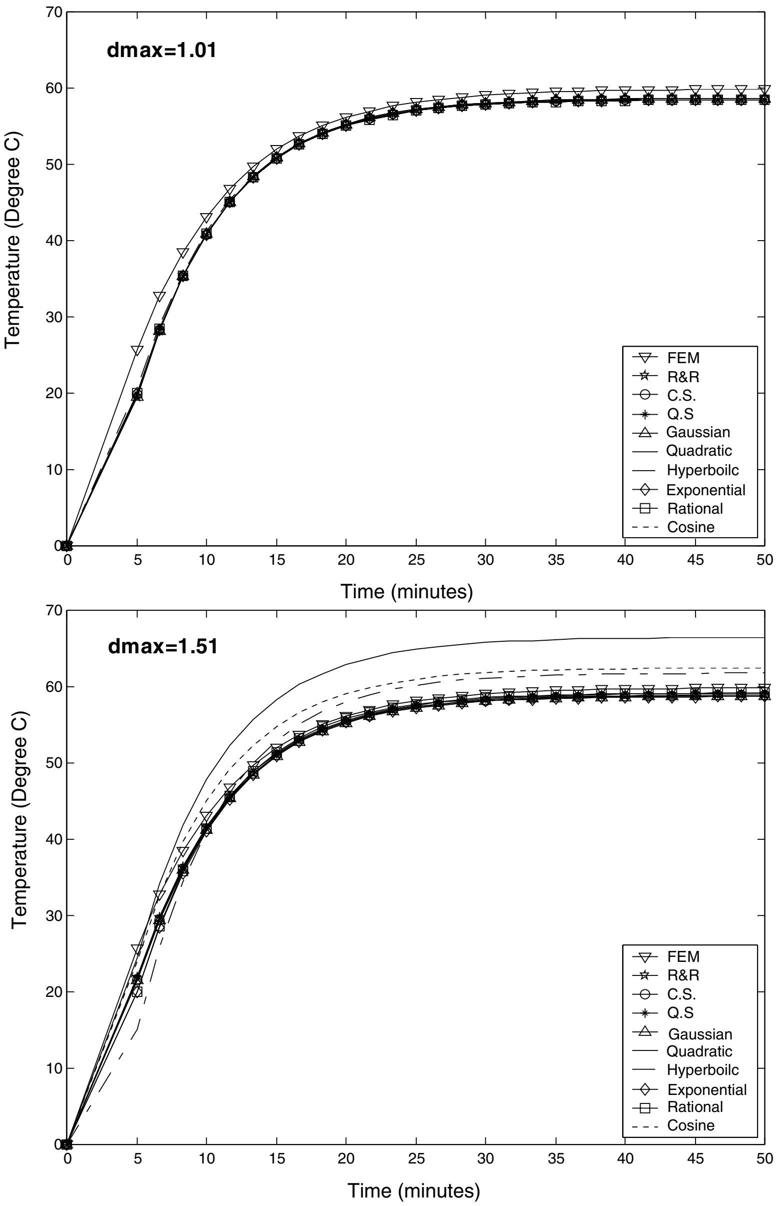

Fig. 5. Comparison of EFG results obtained using 144 nodes with FEM at the location ($x = 0.6$, $y = 0$ and $z = 0.2$).

Using Eqs. (15c) and (15d) to enforce essential boundary conditions, the functional $I^*(T)$ is obtained as

$$I^*(T) = \sum_{i=1}^{2} \int_{V_i} \left[\frac{1}{2}k_i(\nabla^{\mathrm{T}}T)\nabla T - T\dot{Q}_i + \rho_i c_i T\dot{T}\right] \mathrm{d}V + \sum_{j=1}^{10} \int_{S_j} \frac{hT^2}{2}\,\mathrm{d}S - \sum_{j=1}^{10} \int_{S_j} hTT_\infty\,\mathrm{d}S + \sum_{i=1}^{2} \int_{S_{i\mathrm{F}}} \lambda(T - T_{S_{i\mathrm{F}}})\,\mathrm{d}S. \tag{20}$$

Using variational method, Eq. (20) reduces to

$$\delta I^*(T) = \sum_{i=1}^{2} \int_{V_i} [k_i(\nabla^{\mathrm{T}}T)\delta\nabla T - \dot{Q}_i\delta T + \rho_i c_i \dot{T}\delta T]\,\mathrm{d}V + \sum_{j=1}^{10} \int_{S_j} hT\delta T\,\mathrm{d}S - \sum_{j=1}^{10} \int_{S_j} hT_\infty \delta T\,\mathrm{d}S + \sum_{i=1}^{2} \int_{S_{i\mathrm{F}}} [\lambda\delta T + \delta\lambda(T - T_{S_{i\mathrm{F}}})]\,\mathrm{d}S. \tag{21}$$

Since δT and $\delta\lambda$ are arbitrary in preceding Eq. (21), the following equations are obtained using Eqs. (8) and (21):

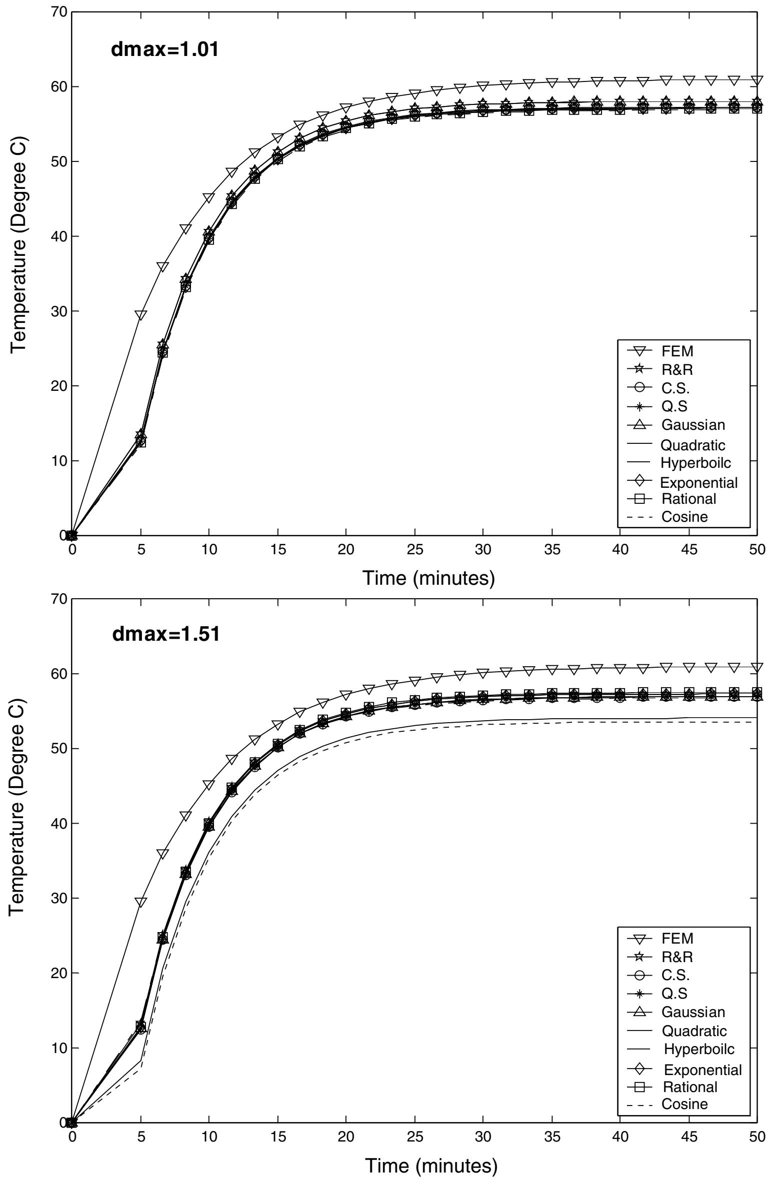

Fig. 6. Comparison of EFG results obtained using 96 nodes with FEM at the location ($x = 0.6$, $y = 0$ and $z = 0.3$).

$$[\mathbf{K}]\{\mathbf{T}\} + [\mathbf{C}]\{\dot{\mathbf{T}}\} + [\mathbf{G}]\{\boldsymbol{\lambda}\} = \{\mathbf{f}\}, \tag{22a}$$

$$[\mathbf{G}^{\mathrm{T}}]\{\mathbf{T}\} = \{\mathbf{q}\}, \tag{22b}$$

$$K_{IJ} = \sum_{i=1}^{2} \int_{V_i} \begin{bmatrix} \Phi_{I,x} \\ \Phi_{I,y} \\ \Phi_{I,z} \end{bmatrix}^{\mathrm{T}} \begin{bmatrix} k_i & 0 & 0 \\ 0 & k_i & 0 \\ 0 & 0 & k_i \end{bmatrix} \begin{bmatrix} \Phi_{I,x} \\ \Phi_{I,y} \\ \Phi_{I,z} \end{bmatrix} \mathrm{d}V + \sum_{j=1}^{10} \int_{S_j} h\Phi_I^{\mathrm{T}}\Phi_J \,\mathrm{d}S, \tag{23a}$$

$$C_{IJ} = \sum_{i=1}^{2} \int_{V_i} \rho_i c_i \Phi_I^{\mathrm{T}} \Phi_J \,\mathrm{d}V, \tag{23b}$$

$$f_I = \sum_{i=1}^{2} \int_{V_i} \dot{Q}_i \Phi_I \,\mathrm{d}V + \sum_{j=1}^{10} \int_{S_j} hT_\infty \Phi_I \,\mathrm{d}S, \tag{23c}$$

$$G_{IK} = \int_{S_{1F}} \Phi_I N_K \,\mathrm{d}S + \int_{S_{2F}} \Phi_I N_K \,\mathrm{d}S, \tag{23d}$$

$$q_K = \int_{S_{1F}} T_{S_{1F}} N_K \,\mathrm{d}S + \int_{S_{2F}} T_{S_{2F}} N_K \,\mathrm{d}S. \tag{23e}$$

Using backward difference technique for time approximation, Eq. (22) can be written as

$$\begin{bmatrix} \mathbf{K}^* + \mathbf{C} & \mathbf{G} \\ \mathbf{G}^T & 0 \end{bmatrix} \begin{Bmatrix} \mathbf{T}_{\bar{n}} \\ \boldsymbol{\lambda} \end{Bmatrix} = \begin{Bmatrix} \mathbf{R}_{\bar{n}} \\ \mathbf{q} \end{Bmatrix} \tag{24}$$

where

$$\mathbf{R}_{\bar{n}} = ([\mathbf{C}] - (1-\alpha)\Delta t[\mathbf{K}])\{\mathbf{T}\}_{\bar{n}-1} + \alpha\Delta t\{\mathbf{f}\}_{\bar{n}} + (1-\alpha)\Delta t\{\mathbf{f}\}_{\bar{n}-1}, \tag{24a}$$

$$\mathbf{K}^* = \alpha\Delta t[\mathbf{K}]. \tag{24b}$$

4. Numerical results and discussion

The different parameters used for three-dimensional steady-state and transient analysis of the composite heat transfer model shown in Fig. 1 are tabulated in Table 1. The EFG results are obtained using different weight functions for two sets of nodes. The FEM results are obtained using ANSYS package and 8-noded brick element (SOLID 70) for the same sets of nodes. A comparative study is carried out to evaluate the performance of different EFG weight functions.

4.1. Steady-state analysis

The steady-state EFG results have been obtained using different weight functions for a composite three-dimensional model problem. L_2-error norms of temperature values have been calculated for different EFG weight functions using two sets of nodes. Table 2 shows the L_2-error norms obtained using two values of scaling parameter (i.e. $d_{\max} = 1.01$ and 1.51) for 96 and 144 nodes. From the results presented in Table 2, it has been observed that the results obtained using different EFG weight function are almost identical for $d_{\max} = 1.01$ but for $d_{\max} = 1.51$, only R&R, CS, QS, Gaussian, exponential and rational weight functions give acceptable results. It has also been noticed that the EFG results start converging with the increase in number of nodes.

The effect of scaling parameter ($d_{\max}$) on EFG results obtained using different weight functions is presented in Table 3 for 96 nodes at the location ($x = 0.2$, $y = 0$ and $z = 0.2$) and in Table 4 for 144 nodes at the same location ($x = 0.2$, $y = 0$ and $z = 0.2$). The similar effect of scaling parameter on EFG results has also been shown in Table 5 for 96 nodes at the location ($x = 0.5$, $y = 0$ and $z = 0.1$) and in Table 6 for 144 nodes the same location ($x = 0.5$, $y = 0$ and $z = 0.1$). Fig. 2 shows the effect of scaling parameter on EFG results obtained using 96 and 144 nodes at the location ($x = 0.4$, $y = 0$ and $z = 0.3$). The similar effect of scaling parameter on EFG results is observed in Fig. 3 at the location ($x = 0.6$, $y = 0$ and $z = 0.3$). From tables and figures, it is clear that only R&R, CS, QS, Gaussian, exponential and rational weight functions gives acceptable results in the range $1.0 < d_{\max} < 1.5$ whereas the results obtained using quadratic, hyperbolic and cosine weight functions are varying in abrupt manner with scaling parameter ($d_{\max}$). Therefore EFG results obtained using quadratic, hyperbolic and cosine weight functions are not reliable in the range $1.0 < d_{\max} < 1.5$. It is also observed that there is minimum variation in the EFG results with the increase in the value of scaling parameter ($d_{\max}$) for exponential weight function.

4.2. Transient analysis

The transient analysis of three-dimensional composite model is also carried out using different EFG weight functions. The EFG results have been obtained at few typical locations for two sets of nodes using two values of scaling parameter. Table 7 shows a comparison of temperature values obtained using 96 nodes with FEM results at the location ($x = 0.4$, $y = 0$ and $z = 0.2$) for $d_{\max} = 1.01$. A comparison of temperature values obtained using 96 nodes with FEM results is also presented in Table 8 at the same location ($x = 0.4$, $y = 0$ and $z = 0.2$) for $d_{\max} = 1.51$. Tables 9 and 10 show the similar comparisons of temperature values obtained using 144 nodes for $d_{\max} = 1.01$ and 1.51, respectively at the location ($x = 0.4$, $y = 0$ and $z = 0.2$). Fig. 4 shows the comparison of temperature values obtained using 96 nodes with FEM results for $d_{\max} = 1.01$ and 1.51 at the location ($x = 0.6$, $y = 0$ and $z = 0.2$). The similar comparison of temperature values obtained using 144 nodes with FEM results is shown in Fig. 5 at the same location ($x = 0.6$, $y = 0$ and $z = 0.2$). Fig. 6 shows the comparison of temperature values obtained using 96 nodes with

FEM results for $d_{max} = 1.01$ and 1.51 at another location ($x = 0.6$, $y = 0$ and $z = 0.3$). The similar comparison of temperature values obtained using 144 nodes with FEM results is shown in Fig. 7 at the same location ($x = 0.6$, $y = 0$ and $z = 0.3$). From the results presented in tables and figures, it is clear that the EFG results obtained using different weight functions are almost identical for $d_{max} = 1.01$ but for $d_{max} = 1.51$ only R&R, CS, QS, Gaussian, exponential and rational weight functions give acceptable results. It has also been observed that the results obtained by EFG method are in good agreement with those obtained by FEM and moreover with the increase in number of nodes EFG results starts converging.

5. Conclusions

In the present analysis, the EFG method has been successfully used to obtain the numerical solution of three-dimensional composite heat transfer problems. The MATLAB codes have been developed to obtain the numerical solution for a model problem. The results obtained using different EFG weight functions are

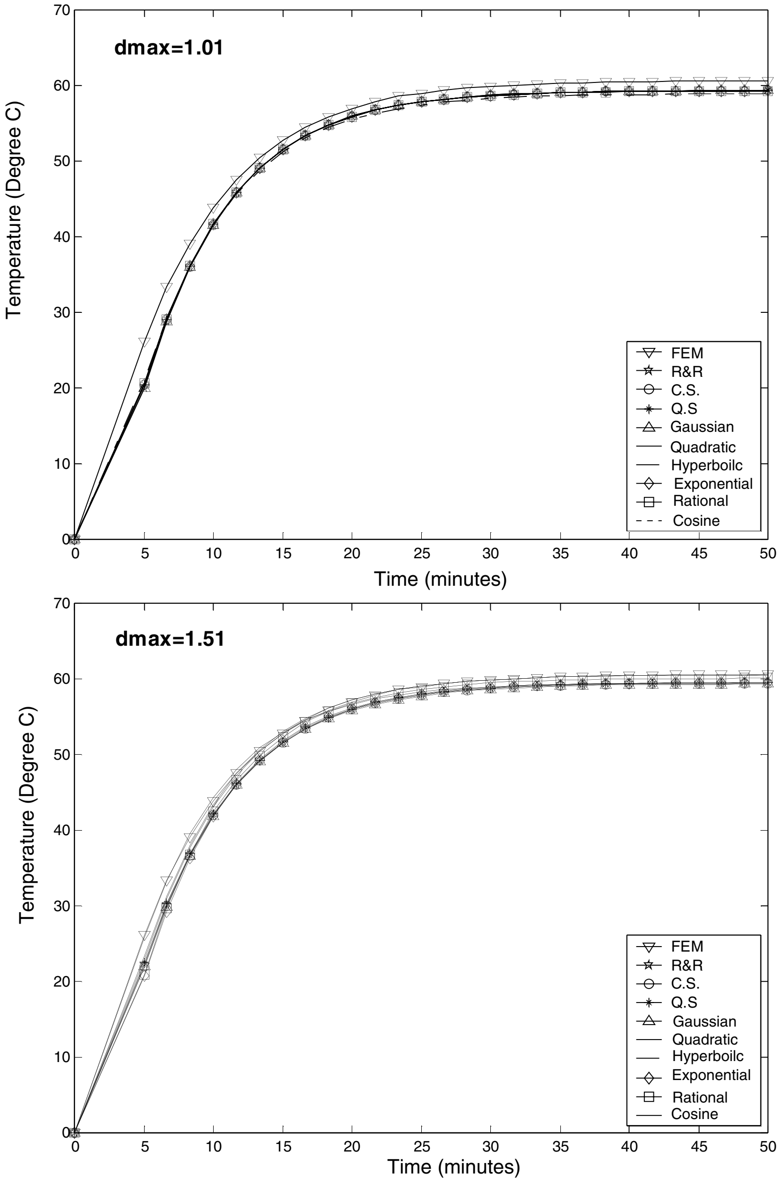

Fig. 7. Comparison of EFG results obtained using 144 nodes with FEM at the location ($x = 0.6$, $y = 0$ and $z = 0.3$).

compared with those obtained by FEM to evaluate the performance of the weight functions. It has been found that the EFG results obtained using proposed (exponential, rational and cosine) and existing (R&R, CS, QS, Gaussian, quadratic and hyperbolic) weight functions are in good agreement with those obtained by FEM. From this analysis, it is clear that only R&R, CS, QS, Gaussian, exponential and rational weight functions give acceptable results in the range $1.0 < d_{\max} < 1.5$. The results obtained using exponential weight function are more reliable as compared to other used weight functions because only exponential weight function has minimum variation in the results with the change in the value of scaling parameter. This work can be extended further for complex three-dimensional problems.

References

[1] J.J. Monaghan, An introduction to SPH, Comput. Phys. Commun. 48 (1988) 89–96.

[2] B. Nayroles, G. Touzot, P. Villon, Generalizing the finite element method: diffuse approximation and diffuse elements, Comput. Mech. 10 (1992) 307–318.

[3] W.K. Liu, S. Jun, Y.F. Zhang, Reproducing kernel particle methods, Int. J. Numer. Meth. Eng. 20 (1995) 1081–1106.

[4] I. Babuska, J.M. Melenk, The partition of unity method, Int. J. Numer. Meth. Eng. 40 (1997) 727–758.

[5] G. Yagawa, T. Yamada, Free mesh method: a new meshless finite element method, Comput. Mech. 18 (1996) 383–386.

[6] T. Belytschko, Y.Y. Lu, L. Gu, Element free Galerkin methods, Int. J. Numer. Meth. Eng. 37 (1994) 229–256.

[7] Y.Y. Lu, T. Belytschko, L. Gu, A new implementation of the element free Galerkin method, Comput. Meth. Appl. Mech. Eng. 113 (1994) 397–414.

[8] T. Belytschko, Y. Krongauz, D. Organ, M. Fleming, P. Krysl, Meshless methods: an overview and recent developments, Comput. Meth. Appl. Mech. Eng. 139 (1996) 3–47.

[9] J. Dolbow, T. Belytschko, An introduction to programming the meshless element free Galerkin method, Arch. Comput. Meth. Eng. 5 (1998) 207–241.

[10] W.K. Liu, Y. Chen, C.T. Chang, T. Belytschko, Advances in multiple scale kernel particle methods, Comput. Mech. 18 (1996) 73–111.

[11] Y. Krongauz, T. Belytschko, A Petrov–Galerkin diffuse element method (PG-DEM) and its comparison to EFG, Comput. Mech. 19 (1997) 327–333.

[12] W.K. Liu, S. Liu, T. Belytschko, Moving least square kernel Galerkin method: methodology and convergence, Comput. Meth. Appl. Mech. Eng. 13 (1997) 113–154.

[13] W.K. Liu, S. Hao, T. Belytschko, S. Li, C.T. Chang, Multiple scale meshfree methods for damage fracture and localization, Comput. Mater. Sci. 16 (1999) 197–205.

[14] T. Belytschko, Y. Krongauz, J. Dolbow, C. Gerlach, On the completeness of meshfree particle methods, Int. J. Numer. Meth. Eng. 43 (1998) 785–819.

[15] T. Zhu, J.D. Zhang, S.N. Atluri, A meshless local boundary integral equation (LBIE) method for solving nonlinear problems, Comput. Mech. 22 (1998) 174–186.

[16] S.N. Atluri, T. Zhu, A new meshless local Petrov–Galerkin (MLPG) approach in computational mechanics, Comput. Mech. 22 (1998) 117–127.

[17] N. Sukumar, B. Moran, T. Belytschko, The natural element method in solid mechanics, Int. J. Numer. Meth. Eng. 43 (1998) 839–887.

[18] S. De, K.J. Bathe, The method of finite spheres, Comput. Mech. 25 (2000) 329–345.

[19] N. Sukumar, B. Moran, A. Yu Semenov, V.V. Belikov, Natural neighbor Galerkin methods, Int. J. Numer. Meth. Eng. 50 (2001) 1–27.

[20] T. Belytschko, L. Gu, Y.Y. Lu, Fracture and crack growth by element-free Galerkin methods, Model. Simul. Mater. Sci. Eng. 2 (1994) 519–534.

[21] N. Sukumar, B. Moran, T. Black, T. Belytschko, An element-free Galerkin method for three-dimensional fracture mechanics, Comput. Mech. 20 (1997) 170–175.

[22] T. Belytschko, Y.Y. Lu, L. Gu, M. Tabbara, Element-free Galerkin methods for static and dynamic fracture, Int. J. Solids Struct. 32 (1995) 2547–2570.

[23] T. Belytschko, M. Tabbara, Dynamic fracture using element-free Galerkin methods, Int. J. Numer. Meth. Eng. 39 (1996) 923–938.

[24] Y.Y. Lu, T. Belytschko, M. Tabbara, Element-free Galerkin methods for wave propagation and dynamic fracture, Comput. Meth. Appl. Mech. Eng. 126 (1995) 131–153.

[25] T. Belytschko, Y.Y. Lu, L. Gu, Crack propagation by element-free Galerkin methods, Engineering Fracture Mechanics 51 (2) (1995) 295–315.

[26] P. Krysl, T. Belytschko, Analysis of thin plates by element-free Galerkin method, Comput. Mech. 17 (1996) 26–35.

[27] P. Krysl, T. Belytschko, Analysis of thin shells by element-free Galerkin method, Int. J. Solids Struct. 33 (1996) 3057–3080.

[28] L. Xuan, Z. Zeng, B. Shanker, L. Udpa, A meshless element-free Galerkin method in NDT applications, in: 28th Annual Review of Progress in Quantitative Nondestructive Evaluation, Maine, USA, July 2001, Published in AIP Conference Proceeding.

[29] V. Cingoski, N. Miyamoto, H. Yamashita, Element-free Galerkin method for electromagnetic field computations, IEEE Trans. Magnet. 34 (1998) 3236–3239.

[30] G. Li, T. Belytschko, Element-free Galerkin method for contact problems in metal forming analysis, Eng. Comput. 18 (2001) 62–78.

[31] I.V. Singh, K. Sandeep, R. Prakash, Heat transfer analysis of two-dimensional fins using meshless element-free Galerkin method, Numer. Heat Transfer—Part A 44 (2003) 73–84.

[32] I.V. Singh, K. Sandeep, R. Prakash, The element free Galerkin method in three dimensional steady state heat conduction, Int. J. Comput. Eng. Sci. 3 (3) (2002) 291–303.

[33] S. Rahman, B.N. Rao, A perturbation method for stochastic meshless analysis in elastostatics, Int. J. Numer. Meth. Eng. 50 (8) (2001) 1969–1991.

[34] S. Rahman, B.N. Rao, An element free Galerkin method for probabilistic mechanics and reliability, Int. J. Solids Struct. 38 (50–51) (2001) 9313–9330.

[35] P. Lancaster, K. Salkauskas, Surfaces generated by moving least square methods, Math. Comput. 37 (1981) 141–158.
[36] P. Krysl, T. Belytschko, ESFLIB: a library to compute the element free Galerkin shape functions, Comput. Meth. Appl. Mech. Eng. 190 (2001) 2181–2205.
[37] T. Zhu, S.N. Atluri, A modified collocation method and a penalty formulation for enforcing the essential boundary conditions in the element free Galerkin method, Comput. Mech. 21 (1998) 211–222.
[38] Y. Krongauz, T. Belytschko, Enforcement of essential boundary conditions in meshless approximation using finite elements, Comput. Meth. Appl. Mech. Eng. 131 (1996) 1335–1345.
[39] I. Kaljevic, S. Saigal, An improved element free Galerkin formulation, Int. J. Numer. Meth. Eng. 40 (1997) 2953–2974.
[40] B.N. Rao, S. Rahman, An efficient meshless method for fracture analysis of cracks, Comput. Mech. 26 (2000) 398–408.